A Power Supply of Self-Powered Online Monitoring Systems for Power Cords

Zhiyi Wu, Yumei Wen, and Ping Li

***Abstract*—This paper presents a power supply of self-powered online monitoring systems for power cords. The proposed power supply obtains energy from the magnetic field induced by wire-carrying currents using a specially designed coil-based magnetic energy harvester (CMEH). The CMEH reduces the influence of the magnetic flux leakage and can harvest enough energy, especially when the wire-carrying current is small. The magnetic core of the CMEH contains two special C-cores and all end faces are tooth profile. The relationship between the magnetic flux leakage and the number of teeth has been analyzed. The design details of the power supply circuit including the unit for power management and overvoltage protection are given in this paper. Test results show that the overvoltage protective unit can protect the supercapacitor from over its max operating voltage. With the low dropout regulator unit function, the power supply is capable of providing a stable output voltage.**

***Index Terms*—Low dropout regulator, magnetic energy harvester, magnetic flux leakage, online monitoring system, power cord, power supply.**

I. Introduction

With extensive applications of appliances in factories, hospitals, schools, etc., there appears a growing demand of electricity consumption. In order to avoid fires and other disasters and ensure the safety of electricity, monitoring real-time online condition of power cords is becoming critical. Due to the fact that the monitoring system is expected to continuously work for a long time and without maintenance, using the battery as the power source will not be able to meet requirements. A promising solution alternative to batteries is the use of energy harvesting devices that convert ambient energies into electricity.

The study of monitoring real-time online condition of wires first has been developed in high-voltage transmission lines. Researchers have proposed some online monitoring methods addressing the measurement of condition parameters of transmission lines [1]–[4]. However, the power sources for monitoring systems have continued to be a challenging problem. The most common way is to harvest solar energy by using the solar cells that have been used in actual applications [5], [6]. But, a strong dependence on the weather conditions greatly reduces the feasibility of harvesting solar energy as the power supply for monitoring systems. Powering active optical current transducers through laser has also been proposed [7]–[9], whereas this method costs highly and laying fiber is too many troubles in engineering applications. In addition, from the capacitor's principle, an electric energy harvester tube has been used to harvest the electrical energy from the overhead power line for powering monitoring systems [10], [11], but the volume of the electric energy harvester is larger than that of a coil-based magnetic energy harvester (CMEH), and a much high voltage of the transmission lines is the precondition for the electric energy harvester harvesting enough energy to drive a monitoring system [11]. The CMEH is also capable of obtaining power energy from overhead current-carrying conductors. In this scheme, a coil is mounted around a wire to supply electric power by transferring the energy from the primary side (the conductor) to the secondary side [12]–[15]. As the primary current, which actually is the carry-on current in a transmission line, is usually very large (at least 100 A), the output voltage of the coil is strong enough to drive a monitoring system. In case, abnormal large primary currents cause overvoltages at the secondary side of the coil. To protect the monitoring system from possible overvoltages, an overvoltage protective circuit is employed [12], [13]. In order to ensure the CMEH can be able to provide stable outputs in a wide primary current range, an air gap is added to the magnetic core to increase the magnetic reluctance of the core path [13].

In the study of CMEHs, the relevant research results promote them into practice for powering the monitoring systems of transmission lines. In the case of power cords, the carrying-on current and voltage usually are much smaller than those of the transmission line, so the output power of the CMEH may not be sufficient for the monitoring systems. Thus, there still need further work to promote the CMEH to provide power for the monitoring systems of power cords. In addition, in UC Berkley, researchers also proposed a piezoelectric magnetic energy harvester to harvest the magnetic energy surrounding power cords for powering wireless sensor nodes [16]–[18], whereas this method is an alternative to CMEHs in cases where the harvesters cannot encircle the cord [18]. To avoid cutting off the cord first when installing the CMEH, Ahola *et al.* [19] used a CMEH with the core consisted of two U-cores as the power supply of the on-line condition monitoring system for electric motors. For harvesting more energy to increase the output power, researchers usually increase the size of a core, use the magnetic material with high permeability to fabricate a core [20], or connect the output of many

Manuscript received January 23, 2013; revised August 5, 2013; accepted September 4, 2013. Date of publication October 21, 2013; date of current version November 20, 2013. This work was supported by the National Natural Science Foundation of China (No. 61071042), Higher School Specialized Research Fund for the Doctoral Program No. 20100191110009 and the Graduate Innovation Foundation of Chongqing University (No. CDJXS11120006). Paper no. TEC-00037-2013.

The authors are with the Department of Optoelectronic Engineering, Chongqing University, Chongqing 400044, China (e-mail: wuzhiyi@cqu.edu.cn; ymwen@cqu.edu.cn; liping@cqu.edu.cn).

Color versions of one or more of the figures in this paper are available online at http://ieeexplore.ieee.org.

Digital Object Identifier 10.1109/TEC.2013.2281075

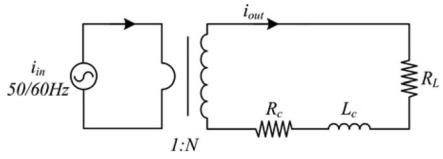

Fig. 1. Equivalent on-load model of a CMEH.

CMEHs in parallel [19]. However, due to the existence of air gap at the openness even when the magnetic core is shut up, the magnetic flux leakage increases dramatically, then causes the output power of the harvester to decrease significantly [20]. The magnetic flux leakage from the air gap in an open core has been showed by the effective magnetic permeability's theoretical expression and the three-dimensional (3-D) finite element method (FEM) simulation results [21]. So, reducing the magnetic flux leakage is vital to the increasing of output power. Thus, further investigation on design of a magnetic core to reduce the magnetic flux leakage is necessary to promote the CMEH power supplies also into practice for powering the online monitoring systems of power cords. Additionally, to ensure the CMEH can provide a stable output power, a power management circuit including power regulator module, protective module and so on is indispensable. The output voltage of the CMEH is rectified and filtered to obtain a dc voltage. Then, the dc voltage is interfaced by a step-down dc converter to get a stable 5 V output voltage [13]. This method is suitable for the case where the output voltage of the CMEH is large enough. When the output voltage of the CMEH is small, the dc voltage usually has been used to charge an energy storage module [15], [20]. However, unlike some other power management circuits in which the energy storage module also has been used [22], for CMEH, the overvoltage protective must be introduced into the power management in case the energy storage module is charged to over its max operating voltage.

In this paper, a specially designed CMEH with tooth profile core has been proposed. The core contains two special C-cores and all end faces are tooth profile. Compared with the core with two traditional C-cores, it can significantly reduce the magnetic flux leakage in times with the dimensions remaining the same. And then, to generate stable power from the CMEH power supply, a power management unit based on a supercapacitor and a low dropout regulator (LDO) module has been developed. An overvoltage protective unit has been exploited to protect the supercapacitor from over its max operating voltage. The test results are given and analyzed in this paper as well.

II. Design Principle of the CMEH

A. Theoretical Analysis

Fig. 1 shows the fundamental on-load operating principle of a CMEH, which is similar to a current transformer. In the harvester, the primary side is passed by ac current and is a one-turn winding.

According to the electromagnetic theory, the magnetic flux density B_w at a radial distance r from the center of a single conductor wire of infinite length carrying-on current $i_{\rm in}$ is calculated as follows:

$$B_w = \mu_0 H_w = \frac{\mu_0 i_{\rm in}}{2\pi r}. \tag{1}$$

In (1), H_w is the intensity of magnetic field, μ_0 is the permeability of free space, equals to $4\pi \times 10^{-7}$ H/m. The magnetic field is directed circumferentially around the wire using the "right-hand rule." Equation (1) shows that the magnetic field intensity is directly proportional to the current in the wire and inversely proportional to the distance from the wire. For a wire carrying an alternating current, the intensity and direction of the magnetic field will vary in phase with the current.

When a CMEH is installed around the single conductor wire, the average magnetic flux density $\bar{B}_w$ of the magnetic core induced by $i_{\rm in}$ can be written as

$$\bar{B}_w = \frac{1}{w}\int_{r_{\rm in}}^{r_{\rm in}+w} \mu_0\mu_r H_w\, dr = \frac{\mu_0\mu_r i_{\rm in}}{2\pi w}\ln\left(\frac{r_{\rm in}+w}{r_{\rm in}}\right) \tag{2}$$

where μ_r is the relative permeability and $r_{\rm in}$ and w are the inner radius and the width of the core, respectively.

When the magnetic circuit is closed, the effect of the secondary magnetic field induced by the coil's output current $i_{\rm out}$ cannot be ignored. Based on the Ampere's circuital theorem, the average secondary magnetic flux density $\bar{B}_c$ of the magnetic core is represented as follows:

$$\bar{B}_c = \frac{1}{w}\int_{r_{\rm in}}^{r_{\rm in}+w} \mu_0\mu_r \frac{N i_{\rm out}}{2\pi r}\, dr = \frac{\mu_0\mu_r N i_{\rm out}}{2\pi w}\ln\left(\frac{r_{\rm in}+w}{r_{\rm in}}\right). \tag{3}$$

On the basis of the Lenz's law, the effective average magnetic flux density can be obtained as

$$\bar{B}_{\rm eff} = \bar{B}_w - \bar{B}_c = \frac{\mu_0\mu_r}{2\pi w}\ln\left(\frac{r_{\rm in}+w}{r_{\rm in}}\right)(i_{\rm in} - N i_{\rm out}). \tag{4}$$

As the coil's induced electromotive force ξ is defined as

$$\xi = \frac{-d\Psi}{dt} = \frac{-N d\Phi}{dt} \tag{5}$$

where Ψ is the flux linkage, $\Phi = BS$ is the magnetic flux, S is the flux area, and N is the coil turn number. So substituting (4) into (5), ξ can be rewritten as

$$\xi = -\frac{\mu_0\mu_r N h}{2\pi}\ln\left(\frac{r_{\rm in}+w}{r_{\rm in}}\right)\left(\frac{di_{\rm in}}{dt} - N\frac{di_{\rm out}}{dt}\right). \tag{6}$$

When the CMEH is connected with a load resistance R_L, on the theory of the Ohm's law, the output current $i_{\rm out}$ is given by

$$i_{\rm out} = \frac{\xi}{j\omega L_c + R_c + R_L} \tag{7}$$

where R_c and L_c are the internal resistance and inductance of coil, respectively.

Assuming $i_{\rm in} = I_{\rm in}\sin(\omega t)$, ω is the angular frequency, $I_{\rm in}$ is the amplitude of $i_{\rm in}$. We can get a first-order linear nonhomogeneous differential equation of $i_{\rm out}$

$$\frac{di_{\rm out}}{dt} - \frac{R}{NA} i_{\rm out} = \frac{\omega I_{\rm in}}{N}\cos(\omega t) \tag{8}$$

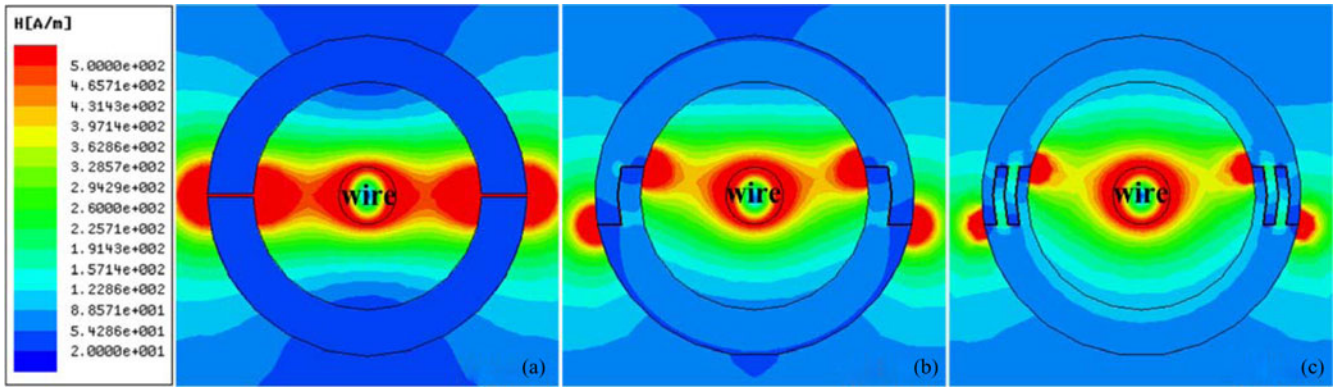

Fig. 2. Magnetic field distribution for magnetic cores with different number of teeth. (a) The core of two traditional C-cores, denoted as 0 tooth, (b) 2 teeth, and (c) 4 teeth.

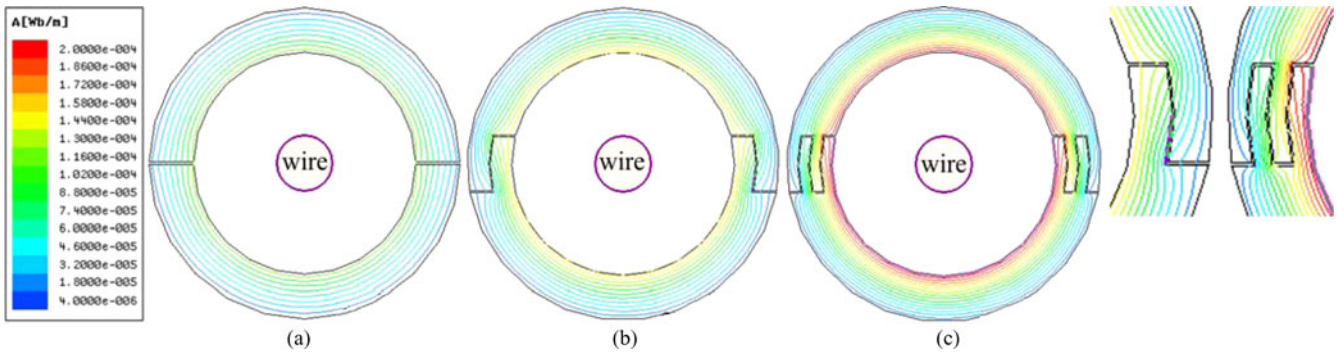

Fig. 3. Magnetic force lines distribution for magnetic cores with different number of teeth: (a) 0 tooth, (b) 2 teeth, and (c) 4 teeth.

hence, we have

$$i_{\text{out}} = \frac{A\omega I_{\text{in}}}{\sqrt{R^2 + A^2N^2\omega^2}} \sin(\omega t + \varphi) \tag{9}$$

where $\cos\varphi = AN\omega/\sqrt{R^2 + A^2N^2\omega^2}$, $R = j\omega L_c + R_c + R_L$, and $A = \mu_0\mu_r Nh\ln((r_{\text{in}} + w)/r_{\text{in}})/2\pi$. The amplitude of i_{out} is I_{out}, and equals to $A\omega I_{\text{in}}/\sqrt{R^2 + A^2N^2\omega^2}$.

The relative permeability μ_r is measured when the specimen is in the "cyclic magnetic state" [23], such as a closed ring shape magnetic core. But, due to the influence of shape demagnetizing effect and magnetic flux leakage, magnetic flux density in the core with an air gap decreases. Hence the nominal relative permeability is not eligible applied in (9). Here the effective permeability should be filled in, which is the ratio of the actual magnetic induction and the applied field in this case.

From (9), we can know that the output current is directly proportional to the permeability, height and width of the magnetic core, and is inversely proportional to the magnetic core's inner radius. When the core's dimensions and coil winding is specified, for harvesting more energy, the permeability of the magnetic core has to be increased. Usually, researchers use a magnetic material with high permeability to fabricate cores. But when magnetic cores have an air gap, magnetic flux leakage increases, which, in turn, greatly reduces the actual magnetic flux within the core. The effective permeability cannot be increased significantly by using a high permeability magnetic material.

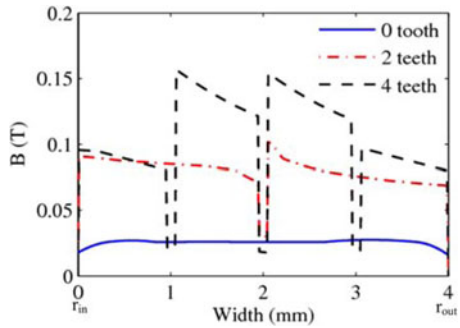

Fig. 4. Magnetic induction B distribution at the teeth along the core's width direction.

Thus, the following research aims to reduce the magnetic flux leakage for increasing the output power of the CMEH.

B. Magnetic Flux Leakage of Different Cores

To reduce the magnetic flux leakage, we proposed a magnetic core contains two special C-cores and all end faces are tooth profile. The magnetic performances of the proposed magnetic core have been analyzed by Maxwell software and the results are shown in Figs. 2–5. Fig. 2 shows the magnetic field distribution for cores with different number of teeth. With the increase of the number of teeth, the magnetic flux leakage reduces obviously, as shown in the red region around the gap. Meanwhile, the magnetic force lines are getting more concentrated within the core,

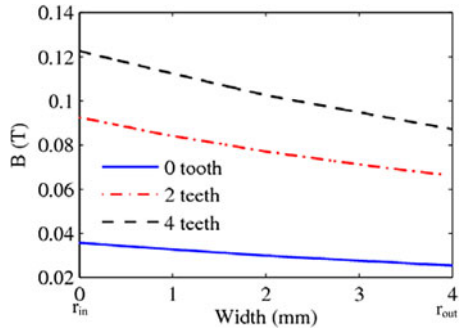

Fig. 5. Magnetic induction B distribution at the arm along the core's width direction.

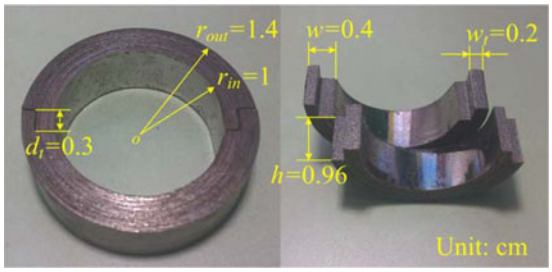

Fig. 6. Proposed core: w, h, and $r_{\rm in}$ and $r_{\rm out}$ are the width, height, and inner and outer radii of the core, respectively, and w_t and d_t are the width and depth of the teeth.

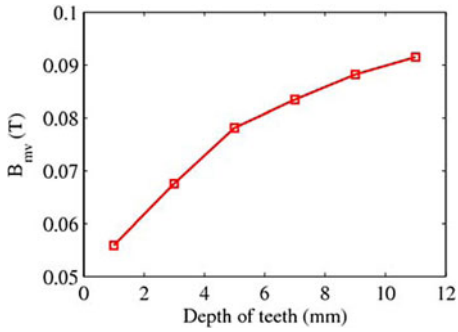

Fig. 7. Mean values of the magnetic induction intensity (B_{mv}) at the arm along the core's width direction for the cores with different depth of teeth.

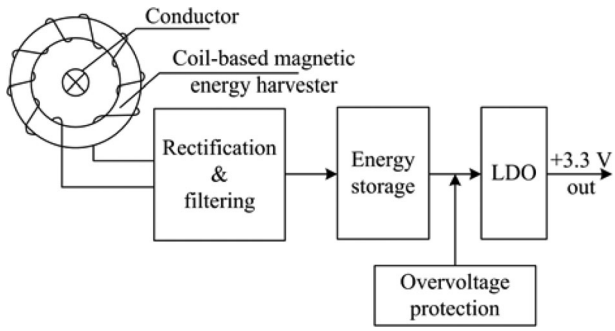

Fig. 8. Schematic of the CMEH power supply.

as shown in Fig. 3. The reason is that according to the analysis of magnetic circuit, the magnetic force line tends to converge in the path with a smaller magnetic reluctance, as shown in the detail of Fig. 3. Thus, when the number of teeth increases, the magnetic flux raises too. As the cross sections of those cores are the same, so the magnetic induction is directly proportional to the number of teeth. Fig. 4 shows the magnetic induction distribution at the teeth along the core's width direction. With increasing of the number of teeth, the magnetic induction intensity in the teeth is improved significantly. The coil is wound around the core's arm. Then, the magnetic induction distributions at the arm for cores with different number of teeth are shown in Fig. 5. Compared with the core of two traditional C-cores (denoted as 0 tooth), the average magnetic induction of the proposed cores with 2 teeth and 4 teeth are increased by more than 2 and 3 times, respectively. In the analysis, the radius of the power cord is 2.5 mm, the current transmitting through the cord is 10 Arms with 50 Hz, and the dimensions of magnetic cores are shown in Fig. 6.

C. Magnetic Core Design

The magnetic core of the proposed harvester contains two special C-cores and all end faces are tooth profile, as shown in Fig. 6. In designing and fabricating the proposed magnetic core, we first wind a FeSiB ribbon with the thickness of 28 μm into an annulus, then adhere and form the annulus by an epoxy resin, and finally cut the annulus into two special C-cores by wire electrical discharge machining (WEDM). In the process of WEDM, the diameter of the molybdenum wire should be as small as possible. For a close contact of two C-cores, the diameter is much smaller, the two special C-cores can joint much more closely, so the air gap in the proposed core should be much smaller too.

With the increase of the number of the teeth, the effect of reducing the magnetic flux leakage is more significant but with a slow growth in magnetic induction intensity, furthermore, the demands of processing and packaging are getting more complicated and costly. Thus, no matter how much the size of the core, the number of teeth usually is specified as 2. For different depth of the teeth, the mean values of the magnetic induction intensity (B_{mv}) at the arm along the core's width direction have been simulated and plotted in Fig. 7. B_{mv} is direct proportion to the depth of teeth, but B_{mv} per unit depth and the depth of teeth presents an inverse proportion. So, the depth of the teeth should be specified as 1–2 times of the core's width.

III. Power Supply Circuit Implementation

A. Power Supply Circuit

The circuit block diagram of the CMEH power supply (CMEHPS) is shown in Fig. 8. The output voltage of the CMEH is rectified and filtered to obtain a dc voltage output. Then, the dc voltage is used to charge an energy storage module. Finally, a channel of +3.3 V is obtained by an LDO module. A supercapacitor has the advantage of long cycle life, large capacitance, small leakage current, and low equivalent series resistance (ESR) [24]. So it has been used to construct the energy storage module. A max operating voltage exists in the supercapacitor. An overvoltage protective unit is developed to prevent the supercapacitor from being charged to over its max operating voltage.

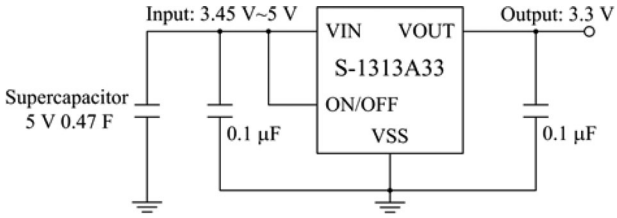

Fig. 9. Circuit of the central power management unit.

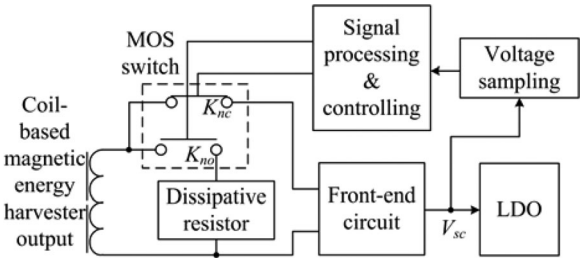

Fig. 10. Block diagram of the overvoltage protective unit.

B. Central Power Management

In the central power management unit (shown in Fig. 9), a supercapacitor with 0.47 F (Cooper Bussmann PowerStor Supercapacitor PB Series) is used as the energy storage module. The working voltage of the supercapacitor is 5 V. To obtain a 3.3 V stable output voltage, a super low current consumption low dropout CMOS voltage regulator S-1313A33 (Seiko Instruments Inc.) is employed. According to the characteristics of S-1313A33, in order to ensure the output current is no less than 100 mA, the input voltage is at least 3.45 V. So the input voltage of S-1313A33 is specified in the range of 3.45 V to 5 V.

C. Overvoltage Protective Unit

In Fig. 10, a monitoring and protective unit is used to protect the supercapacitor from being charged over its max operating voltage. The front-end circuit contains the rectification & filtering unit and the energy storage unit shown in Fig. 8. In order to reduce the power consumption, the MOS switch unit is consisted of four N-channel enhancement mode field-effect transistors (3055 L). The normally open switch $K_{\rm no}$ connects the coil to a dissipative resistor, and the normally closed switch K_{nc} connects the coil to the power supply circuits. The signal processing and controlling unit is exploited for monitoring the voltage of the supercapacitor V_{sc} and controlling the state of K_{nc} and $K_{\rm no}$. When V_{sc} exceeds the max operating voltage of the supercapacitor, the K_{nc} is opened while the $K_{\rm no}$ is closed. By this means, the supercapacitor is protected from the overvoltage condition.

IV. Test Results and Discussion

A. Output Characteristics of CMEH

We fabricated the special C-core that has 2 teeth, as shown in Fig. 6. For comparison, the core of two traditional C-cores also has been fabricated. The dimensions of the two kinds of core are the same. The CMEHs consisted with the two kinds of core are denoted as 0-tooth and 2-teeth, respectively. The relationship between the output current and the load resistance with $N = 2000$ and $I_{\rm in} = 10$ Arms for the 0-tooth and the 2-teeth are shown in Fig. 11. The output current is inversely proportional to the load resistance, and the output current of the 2-teeth is larger than that of the 0-tooth under the same load resistance. That is to say, the ability to drive loads of the proposed harvester is enhanced.

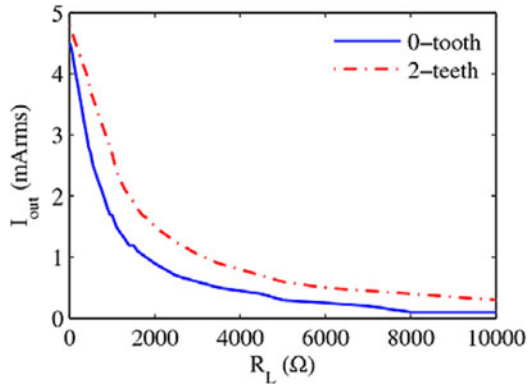

Fig. 11. Output current versus load resistant with $N = 2000$ and $I_{\rm in} = 10$ Arms.

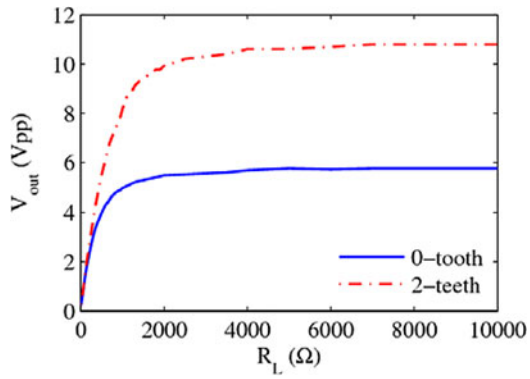

Fig. 12. Output voltage versus load resistant with $N = 2000$ and $I_{\rm in} = 10$ Arms.

Fig. 12 shows the relationship between output voltage and load resistance with $N = 2000$ and $I_{\rm in} = 10$ Arms for the 0-tooth and the 2-teeth. The output voltage increases rapidly and then tends to a steady value as the load resistance increases. Compared with the 0-tooth, the steady state value of the 2-teeth is increased by about 2 times, and this is in accordance with the analysis result. According to the expression of output power $P_{\rm out} = I_{\rm out} \times V_{\rm out}$, the output power versus load resistance with $N = 2000$ and $I_{\rm in} = 10$ Arms for the 0-tooth and the 2-teeth are shown in Fig. 13. The 2-teeth reaches its maximum output power of 63.72 mW and power density of 22.01 mW/cm^3 at $R_L = 750\ \Omega$. Meanwhile, the maximum output power and power density of the 0-tooth are 30.38 mW and 10.49 mW/cm^3 under $R_L = 400\ \Omega$, respectively. Therefore, compared with the 0-tooth, the maximum output power and power density of the proposed harvester both have been increased more than 2 times.

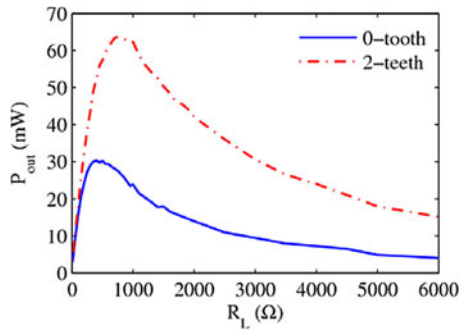

Fig. 13. Output power versus load resistant with $N = 2000$ and $I_{\rm in} = 10$ Arms.

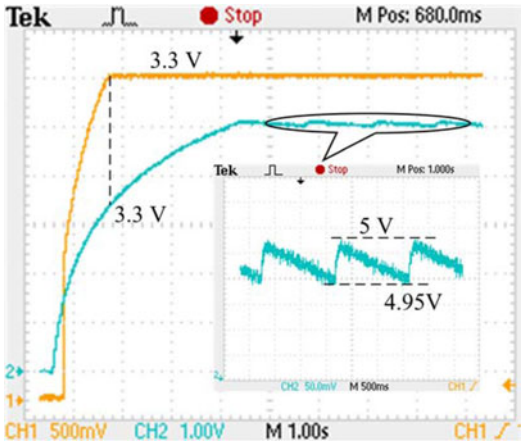

Fig. 14. I/O waveforms of the LDO at the action of the overvoltage protective unit, where CH1 and CH2 symbolize the output and input voltage of the LDO, respectively (CH1: 500 mV/div; CH2: 1 V/div; 1 s/div).

B. I/O Performance Tests

To observe the whole working process of the CMEHPS within a shorter time, an electrolytic capacitor with 470 μF is used to replace the supercapacitor. 470 μF is much smaller than the 0.47 F of the supercapacitor, so the charging speed of the former is much faster under the same conditions. Fig. 14 shows the input and output voltage waveforms of the LDO unit at the action of the overvoltage protective unit. The test results indicate that the LDO unit gives a stable output at 3.3 V when the input voltage $V_{\rm in} > 3.3$ V. The overvoltage protective unit works when $V_{\rm in} > 5$ V and thereby cuts off the circuit behind from the CMEH. And then, the existence of leakage current will inevitably lead to the reduction in the voltage of capacitor. So, when $V_{\rm in} < 4.95$ V, the CMEH should be connected with the following circuit again. Thus, $V_{\rm in}$ finally fluctuates between 4.95 and 5 V, shown in the detail of Fig. 14.

Fig. 15 shows the output waveform of the CMEH at the change of the MOS switch states with $I_{\rm in} = 100$ Arms. When $K_{nc} = 1$ and $K_{\rm no} = 0$ ("1" and "0" represent to the switch is turned off and turned on, respectively), the CMEH is connected with the following circuit, and then the output voltage of the CMEH is clamped to 13.4 $V_{\rm pp}$, which is corresponded to the supercapacitor voltage equals to 4.95 V. When $K_{nc} = 0$ and $K_{\rm no} = 1$, the CMEH is connected with a 5 W 10 Ω dissipative

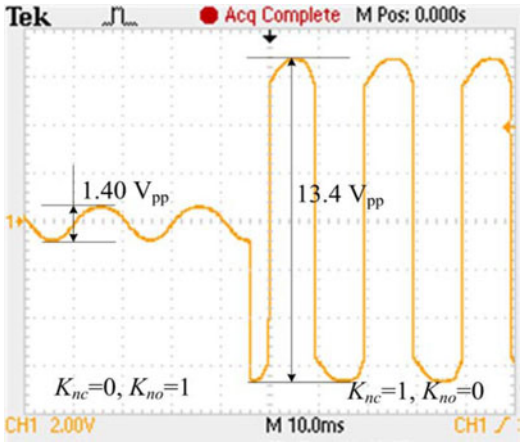

Fig. 15. Output waveform of the CMEH at the change of the MOS switch state with $I_{\rm in} = 100$ Arms (CH1: 2 V/div; 10 ms/div).

resistor, the voltage of which is 1.40 $V_{\rm pp}$ at $I_{\rm in} = 100$ Arms. Then the current through the dissipative resistor is 0.14 A that is much smaller than the maximum current of the dissipative resistor (∼0.71 A). Thus, the maximum input current of the CMEHPS is at least 100 Arms.

To ensure the CMEHPS can provide a steady 3.3 V output voltage with the output current is at least 100 mA, the voltage of the supercapacitor is at least 3.45 V. So the output voltage of the CMEH is clamped to about 9.34 $V_{\rm pp}$, which is smaller than the open-circuit voltage of the CMEH at $I_{\rm in} = 10$ Arms (as shown in Fig. 12). Thus, the minimum input current of the CMEHPS is about 10 Arms. Through optimizing the dimensions and the turn number of the cCMEH, the minimum input current can be further decreased.

As the resistance of the dissipative resistor is only 10 Ω, so the CMEHPS also can be used to measure the carrying-on current of power cords when the CMEH is connected with the dissipative resistor. As shown in Fig. 15, when $I_{\rm in} = 100$ Arms, the current through the dissipative resistor is about 49.5 mArms, then the measured value of $I_{\rm in}$ equals to 99 Arms and the measurement error is 1%.

When the input voltage is larger than 3.3 V, the LDO can gives a stable output at 3.3 V. To ensure the output current of the LDO is no less than 100 mA, the input voltage at least to be 3.45 V. Thus, there is a preparation time before the CMEHPS operating properly.

The traditional CMEH (0-tooth) and the proposed CMEH with 2 teeth (2-teeth) have been used to charge the supercapacitor (5 V 0.47 F), respectively. The relationships between the voltage of the supercapacitor V_{sc} and the time for 0-tooth and 2-teeth with $N = 2000$ and $I_{\rm in} = 20$ Arms are shown in Fig. 16. For charging the supercapacitor to the same V_{sc}, the 2-teeth is faster than the 0-tooth. The time for the V_{sc} equals to 3.3 and 3.45 V of the 0-tooth and 2-teeth are recorded in the subgraph of Fig. 16. Compared with the 0-tooth, the times at $V_{sc} = 3.3$ V and $V_{sc} = 3.45$ V of the 2-teeth are reduced 8 and 13 min, respectively. Therefore, the proposed CMEH can significantly reduce the preparation time of the CMEHPS. In other words,

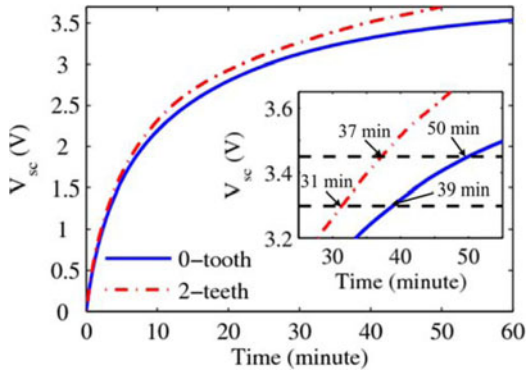

Fig. 16. Voltage of supercapacitor (5 V 0.47 F) versus time with $N = 2000$ and $I_{\text{in}} = 20$ Arms.

TABLE I
BASIC CHARACTERISTICS OF XBEE ZB [27]

RF Data Rate	In -door	Out -door	Supply Voltage	Transmit Current	Receive Current	Power -Down Current
250 Kbps	40m	120 m	2.1~3.6 VDC	35 mA /45mA boost mode @ 3.3VDC	38 mA /40mA boost mode @ 3.3VDC	<1μA @25 °C

the proposed CMEH also can reduce the demand on the input current within the same preparation time.

C. Applications

While the CMEHPS can provide a stable output voltage, with the voltage of the supercapacitor discharging from 5 to 3.45 V, the energy provided by the supercapacitor in the discharging duration is

$$E = \frac{1}{2}V_{sc}^2 C_{sc}\Big|_{3.45\text{V}}^{5\text{V}} = \frac{1}{2} \times \left(5^2 - 3.45^2\right) \times 0.47 \approx 3.08 \text{ J}. \tag{10}$$

The normal efficiency of a regulated power supply circuit is more than 70% [25]. Hence, the energy provided by the CMEHPS is at least 3.08 J × 70% ≈ 2.16 J.

A typically off-the-shelf wireless sensor node current requirement during a transmit/receive operation is 20–50 mA, while during the sleep mode the requirement reduces to only around 10 μA. This implies that the power requirement of most of the node is on the order of several ten milliwatts during the active operation and a few microwatts during the sleep mode [26]. Taking the XBee ZB (Digi International) as an example, its basic characteristics are listed in Table I.

Assume a realistic scenario where a particular wireless sensor node would be required to transmit or receive data once every 10 min or upon occurrence of an event. Also, the total active time for a node is assumed to be around 1 s. So, the power requirement in an operating cycle is

$$\begin{aligned} E_n &\approx 40\,\text{mA} \times 3.3\,\text{V} \times 1\,\text{s} + 1\,\mu\text{A} \times 3.3\,\text{V} \times 10\,\text{min} \\ &= 133.98\,\text{mJ}. \end{aligned} \tag{11}$$

Thus, the 2.16 J provided by the CMEHPS can maintain the XBee ZB working for about 2.69 h.

In each operating cycle, the energy harvested by the CMEH is continuously restored into the supercapacitor. Considering the worst-case scenario when $V_{sc} = 3.45$ V, V_{sc} can be charged to 3.64 V after 10 min, as shown in Fig. 15. So the restored energy in the supercapacitor is about 316.57 mJ. Then, 316.57 mJ × 70% ≈ 221.60 mJ is larger than 133.98 mJ. That is to say, in the operation cycle of the XBee ZB, the restored energy of the CMEHPS can meet the requirement of power consumption. Hence, using the CMEHPS, the XBee ZB can keep working for a long time with the abilities of maintenance-free and self-powered.

As the CMEH contains two special C-cores, so the packaging of it is open-closed type, and the power supply circuit also can be integrated in the same packaging. And then, the CMEHPS is easy to fasten on the power cord. According to the characteristics of the CMEHPS, sensors for detecting temperature, current, and voltage and other sensors used around the power cord such as the smoke detector all could be supplied by the CMEHPS. Sensors, which are small in size, can be integrated with the CMEHPS, while others can be wired connection with the CMEHPS.

V. CONCLUSION

A power supply using a particularly designed CMEH for online wire monitoring systems has been developed and described in this paper. With the help of the CMEH, the proposed power supply can obtain abundant energy directly from the magnetic field induced by wire-carrying currents even when the wire-carrying current is small. Based on theoretical analysis and simulation results, the CMEH with a unique structure containing two special C-cores and all end faces are tooth profile has been developed, which can significantly reduce the magnetic flux leakage in times. Actual tests show that the proposed harvester can provide a maximum power of 63.72 mW under the input current of 10 Arms, which is about 2 times than that of a harvester consisting of two traditional C-cores. In the design details of the power supply circuit, the power management unit and the overvoltage protective unit have been tested and discussed. Test results have indicated that the voltage of the supercapacitor finally fluctuates between 4.95 and 5 V at the action of the overvoltage protective unit. With the LDO unit function, the proposed power supply is capable to supply a stable output voltage at 3.3 V with the output current at least 100 mA. The working range of the CMEHPS is about 10–100 Arms. Moreover, as the resistance of the dissipative resistor is only 10 Ω, so the CMEHPS also can be used to measure the current of power cords when the CMEH is connected with the dissipative resistor. In applications, with the help of CMEHPS, a wireless sensor node such as XBee ZB can keep working for a long time with the abilities of maintenance-free and self-powered.

REFERENCES

[1] E. Fontana, S. C. Oliveira, F. J. M. M. Cavalcanti, R. B. Lima, J. F. Martins-Filho, and E. Meneses-Pacheco, "Novel sensor system for

leakage current detection on insulator strings of overhead transmission lines," *IEEE Trans. Power Del.*, vol. 21, no. 4, pp. 2064–2070, Oct. 2006.
[2] W. Chen, C. Yao, P. Chen, C. Sun, L. Du, and R. Liao, "A new broadband microcurrent transducer for insulator leakage current monitoring system," *IEEE Trans. Power Del.*, vol. 23, no. 1, pp. 355–360, Jan. 2008.
[3] W. de Villiers, J. H. Cloete, L. M. Wedepohl, and A. Burger, "Real-time sag monitoring system for high-voltage overhead transmission lines based on power-line carrier signal behavior," *IEEE Trans. Power Del.*, vol. 23, no. 1, pp. 389–395, Jan. 2008.
[4] S. C. Oliveira, E. Fontana, and F. J. do Monte de Melo Cavalcanti, "Real-time monitoring of the leakage current of 230-kv glass-type insulators during washing," *IEEE Trans. Power Del.*, vol. 24, no. 4, pp. 2257–2260, Oct. 2009.
[5] K. Kobayashi, H. Matsuo, and Y. Sekine, "Novel solar-cell power supply system using a multiple-input DC–DC converter," *IEEE Trans. Ind. Electron.*, vol. 53, no. 1, pp. 281–286, Dec. 2006.
[6] D. Dondi, A. Bertacchini, D. Brunelli, L. Larcher, and L. Benini, "Modeling and optimization of a solar energy harvester system for self-powered wireless sensor networks," *IEEE Trans. Ind. Electron.*, vol. 55, no. 7, pp. 2759–2766, Jul. 2008.
[7] N. A. Pilling, R. Holmes, and G. R. Jones, "Optically powered hybrid current measurement system," *Electron. Lett.*, vol. 29, pp. 1049–1051, Jun. 1993.
[8] T. C. Banwell, R. C. Estes, L. A. Reith, P. W. Shumate, Jr., and E. M. Vogel, "Powering the fiber loop optically-a cost analysis," *J. Lightw. Technol.*, vol. 11, pp. 481–494, Mar. 1993.
[9] K. Goto, T. Nakagawa, O. Nakamura, and S. Kawata, "An implantable power supply with an optically rechargeable lithium battery," *IEEE Trans. Biomed. Eng.*, vol. 48, no. 7, pp. 830–833, Jul. 2001.
[10] H. Zangl, T. Bretterklieber, and G. Brasseur, "Energy harvesting for online condition monitoring of high voltage overhead power lines," in *Proc. 2008 IEEE Instrum. Meas. Technol. Conf.*, Vancouver Island, Canada, 2008, pp. 1364–1369.
[11] H. Zangl, T. Bretterklieber, and G. Brasseur, "A feasibility study on autonomous online condition monitoring of high-voltage overhead power lines," *IEEE Trans. Instrum. Meas.*, vol. 58, no. 5, pp. 1789–1796, May 2009.
[12] L. E. Berkebile, S. Nilsson, and S. Shan, "Digital EHV current transducer," *IEEE Trans. Power App. Syst.*, vol. PAS-100, no. 4, pp. 1498–1504, Apr. 1981.
[13] D. Lin, W. Caisheng, L. Xianzhi, Y. Lijun, M. Yan, and S. Caixin, "A novel power supply of online monitoring systems for power transmission lines," *IEEE Trans. Ind. Electron.*, vol. 57, no. 8, pp. 2889–2895, Aug. 2010.
[14] E. F. Donaldson, J. R. Gibson, G. R. Jones, N. A. Pilling, and B. T. Taylor, "Hybrid optical current transformer with optical and power-line energisation," in *Proc. Inst. Elect. Eng. Gener. Transm. Distrib.*, Sep. 2000, vol. 147, pp. 304–309.
[15] T. Taithongchai and E. Leelarasmee, "Adaptive electromagnetic energy harvesting circuit for wireless sensor application," in *Proc. 6th Int. Conf. Electr. Eng./Electron., Comput., Telecommun. Inf. Technol.*, 2009, pp. 278–281.
[16] E. S. Leland, R. M. White, and P. K. Wright, "Energy scavenging power sources for household electrical monitoring," in *Proc. Power MEMS*, Berkeley, CA, USA, 2006, pp. 165–168.
[17] Q. Xu, R. M. White, I. Paprotny, and P. K. Wright, "Improved performance of nonlinear piezoelectric ac energy scavengers," in *Proc. Power MEMS*, Washington, DC, USA, 2010, pp. 53–56.
[18] I. Paprotny, Q. Xu, W. Chan, R. White, and P. Wright, "Electromechanical energy scavenging from current-carrying conductors," *IEEE Sens. J.*, vol. 13, no. 1, pp. 190–201, Jan. 2013.
[19] J. Ahola, T. Ahonen, V. Sarkimaki, A. Kosonen, J. Tamminen, R. Tiainen, and T. Lindh, "Design considerations for current transformer based energy harvesting for electronics attached to electric motor," in *Proc. Int. Sym. Power Electron., Electr. Drives, Autom. Motion*, 2008, pp. 901–905.
[20] R. H. Bhuiyan, R. A. Dougal, and M. Ali, "A miniature energy harvesting device for wireless sensors in electric power system," *IEEE Sens. J.*, vol. 10, no. 7, pp. 1249–1258, Jul. 2010.
[21] S. Hasanzadeh and S. Vaez-zadeh, "Design of a wireless power transfer system for high power moving applications," *Prog. Electromagn. Res. M*, vol. 28, pp. 258–271, Jan. 2013.
[22] P. Li, Y. Wen, P. Liu, X. Li, and C. Jia, "A magnetoelectric composite energy harvester and power management circuit," *IEEE Trans. Ind. Electron.*, vol. 58, no. 7, pp. 2944–2951, Jul. 2011.
[23] R. M. Bozorth, *Ferromagnetism*. New York, NY, USA: Van Nostrand, 1951, p. 6.
[24] Supercapacitor Cylindrical PB-Series Datasheet. (2013). [Online]. Available: http://www.cooperindustries.com/content/public/en/bussmann/electronics/products/powerstor_supercapacitors/cylindrical/pb-series.html
[25] P. Li, Y. Wen, P. Liu, X. Li, and C. Jia, "A magnetoelectric energy harvester and management circuit for wireless sensor network," *Sens. Actuators A*, vol. 157, pp. 100–106, Jan. 2010.
[26] R. Moghe, Y. Yi, F. Lambert, and D. Divan, "A scoping study of electric and magnetic field energy harvesting for wireless sensor networks in power system applications," in *Proc. IEEE Energy Convers. Congr. Expo.*, 2009, pp. 3550–3557.
[27] XBee ZB Modules Datasheet. (2013). [Online]. Available: http://www.digi.com/pdf/ds_xbeezbmodules.pdf

Authors' photographs and biographies not available at the time of publication.